JOURNAL OF COMPUTATIONAL PHYSICS 105, 207–223 (1993)

The Application of Preconditioning in Viscous Flows

Y.-H. CHOI

Sverdrup Technology, Inc., NASA Lewis Research Center, Cleveland, Ohio 44135

AND

C. L. MERKLE

Department of Mechanical Engineering, The Pennsylvania State University, University Park, Pennsylvania 16802

Received June 20, 1991; revised July 23, 1992

A time-derivative preconditioning algorithm that is effective over a wide range of flow conditions from inviscid to very diffusive flows and from low speed to supersonic flows has been developed. The algorithm uses a preconditioning matrix that introduces well-conditioned eigenvalues while simultaneously avoiding nonphysical time reversals for viscous flows. The resulting algorithm also provides a mechanism for controlling the inviscid and viscous time step parameters at very diffusive flows, thereby ensuring rapid convergence for very viscous flows as well as for inviscid flows. Computational capabilities are demonstrated through computation of a wide variety of problems. Convergence rates are shown to be accelerated by as much as two orders of magnitudes, while providing solutions that are indentical to those obtained without preconditioning method.

1. INTRODUCTION

Time-marching algorithms are widely used for the computation of compressible flows. A major advantage of these techniques is that they apply to both inviscid and viscous flows and can be used in conjunction with virtually any spatial discretization in all Reynolds number regimes. In the past two or three decades, time-marching schemes have been widely accepted and applied as the method of choice for transonic, supersonic, and hypersonic flows.

In the low subsonic Mach number regime, time-marching algorithms do not fare as well. When the magnitude of the flow velocity becomes small in comparison with the acoustic speed, the convective terms of the time-dependent equations become stiff and time-marching methods converge very slowly. These convergence difficulties are then further exacerbated by the magnitude of the diffusion terms, and corrective action can differ substantially when the diffusion terms are missing (the Euler equations), small (high Reynolds numbers) or dominant (low Reynolds numbers). In keeping with the broad applicability of the time-marching method, it is our objective to demonstrate preconditioning methods that eliminate low Mach number convergence difficulties in all Reynolds number regimes.

By way of examples of low Mach number flows, we first note that, if the velocity in the entire flowfield is low, compressibility can be neglected and the stiffness problem can be averted by switching to the incompressible equations. Many problems, however, contain some regions with very low Mach numbers while other regions are decidedly compressible so that the compressible equations must be used throughout. Consequently, one must deal with the stiffness of the equations. Representative problems that contain both compressibility effects and low-speed regions can be grouped into two classes: high-speed flows with embedded regions of low velocity; and low-speed flows with temperature differences arising from strong heat addition. Examples of both are described below.

High-speed flows with embedded regions of low velocity are typified by external, transonic flow with embedded low-speed regions near stagnation points or by choked internal flows with a low velocity region upstream of the choked area. In general, these embedded regions have little effect on convergence when the low-speed region is small, but they can dominate convergence when the size of the region is large. For example, the low-speed region near the stagnation point of an isolated airfoil is seldom large enough to affect convergence, but the subsonic flow upstream of a strongly converging nozzle may completely dominate the convergence process.

Low-speed flows that are compressible because of density changes induced by heat addition can be represented by problems with surface heat transfer or volumetric heat addition. The most common example of volumetric heat addition occurs in combustion problems, but additional problems of interest include advanced space propulsion concepts such as laser, solar, and microwave thermal

0021-9991/93 $5.00

propulsion [1] in which electromagnetic radiation is used to heat a flowing gas. In problems such as these, the equations frequently remain stiff over the entire computational domain so that efficiency requirements make it imperative that the stiffness be dealt with directly.

All of these low speed problems can be encountered in any Reynolds number regime. Several previous researchers have considered the low Mach number problem for inviscid flows. The present paper is directed towards viscous flows.

PREVIOUS WORK ON EIGENVALUE CONTROL

The effect of eigenvalue stiffness on the convergence of both explicit and implicit schemes is well known and two distinct methods have been suggested for controlling the eigenvalues to enhance convergence. The first is to premultiply the time derivative by a suitable matrix that scales the eigenvalues of the system to the same order of magnitude. The other is to use a perturbed form of the equations in which specific terms are dropped such that the physical acoustic waves are replaced by pseudo-acoustic modes. We refer to the former as preconditioning and to the latter as a perturbation procedure. The preconditioning method has the advantage that it provides a global solution that is valid at all Mach numbers, whereas the perturbation method is valid only locally in the regime in which the perturbation is carried out.

A number of preconditioning studies have been reported previously, some dealing with preconditioning in a generalized sense for all flow regimes, while others have focussed on the low Mach number problem. Of the generalized methods, Viviand's [2] was one of the first and one of the most complete. He developed a generalized optimum preconditioning procedure for a class of hyperbolic systems representing the Euler equations and gave specific rules for ensuring that the preconditioned equations remain well posed. The optimum preconditioning matrix is shown to depend upon a preferred direction in space, but even though he presents several specific preconditioning matrices, no general method is available for finding this preferred direction. Additional details concerning preconditioning are presented by Peyret and Viviand [3], who are the only ones so far to consider preconditioning in viscous flows. Turkel [4] also discusses preconditioning with applications to both compressible and incompressible flows and Van Leer *et al.* [5] have used a preconditioning in multi-stage schemes for multi-grid computations. Finally, Storti *et al.* [6] have presented some recent theoretical work on eigenvalue control that agrees well with Viviand's findings. References [2–6] are primarily theoretical in nature and do not include detailed systematic studies of the effectiveness of preconditioning in actual implementations. The present paper deals with the more restricted issue of preconditioning in the low Mach number regime (although examples are given to show that low Mach number issues can dominate stiffness arising from transonic speeds in many practical problems) and proceeds primarily from an implementation viewpoint.

Previous studies of preconditioning in low Mach number inviscid flows have been reported by Briley *et al.* [7] for isoenergetic systems and by the present authors and their co-workers [8–10] for the Euler equations. Low Mach number convergence enhancement by Briley *et al.* was limited to Mach numbers above 0.05. Our results demonstrated that preconditioning provided Mach number independent convergence at all Mach numbers between 0.7 and 10^{-6}. In addition success with "time inclining," which is a simplified form of preconditioning, has been reported by Dannenhoffer and Giles [11].

The second general method for eliminating eigenvalue stiffness is to use a perturbed form of the equations of motion. The present authors [9, 12] have used an expansion of the flow variables in terms of the Mach number squared to remove the physical acoustic waves and replace them by a set of pseudo-acoustic waves whose speeds are comparable to the particle velocity. A similar perturbation procedure has also been developed by Guerra and Gustafsson [13] based upon expansion in Mach number, rather than Mach number squared. This method is extremely effective for both viscous and inviscid flows and has been implemented for numerous applications [14–16]. Other perturbation procedures include the one by Rehm and Baum [17], which is specialized toward combustion problems and has been applied by several authors including Chenoweth and Paolucci [18] and McMurtry *et al.* [19]. Although these perturbation procedures are highly robust and are applicable to both viscous and inviscid flows, the nature of the perturbation limits their usage to low subsonic flows. Specifically, the methods are not adequate for the transonic flow regime and cannot be used for flows that go through the sonic speed. Our focus here is on the preconditioning methods, but we take advantage of knowledge gained from perturbation procedures to develop the preconditioning matrix. One of the goals of the present research is to recover the robustness exhibited by these perturbation schemes in preconditioned methods so that they may be applied through transonic speeds.

To date extension of preconditioning methods to viscous flows has not been reported. We attempted several numerical studies for viscous flows using the preconditioning method of [8, 10] and found that it is not effective in viscous flows. Accordingly, the purpose of the present paper is to develop a method which gives reasonable convergence for all Reynolds number ranges while keeping the same effectiveness in inviscid flows as in the previous method. For the preconditioning matrix to be pertinent for viscous flows, it must not introduce time reversals into the diffusive terms and must maintain well-conditioned inviscid eigenvalues.

To ensure this, we express the equations in terms of a "viscous" set of primary dependent variables, $Q_v = (p, u, v, T)$, which makes it easier to satisfy the diffusive requirements. With these primary dependent variables, the equations degenerate to the classical diffusion equations in the limit of highly diffusive flows and well-conditioned eigenvalues are obtained for the inviscid terms by properly scaling the time derivatives. For the computation of very low Reynolds number flows, additional care must be exercised. Both CFL number and von Neumann number should be kept of order one to obtain efficient convergence. The newly developed algorithm provides a mechanism for controlling these numbers, thereby ensuring rapid convergence for very viscous flows as well as for inviscid flows. The resulting algorithm is effective over a wide range of flow conditions from inviscid to very diffusive flows and from low speed to supersonic flows and the present paper demonstrates the computational capabilities for a wide variety of problems.

As a final note, we address the issue of solution accuracy at low Mach numbers. Volpe [20] showed solutions whose accuracy decreased as the Mach number approached zero, although he gave no explanation for this behaviour. Numerous checks show this deterioration does not occur in our calculations. To the contrary, our compressible solutions approach classical incompressible results more and more closely as the Mach number is reduced. In addition, back-to-back comparisons with results from incompressible codes likewise show the solutions become identical to more and more digits as the Mach number is reduced. We do use roundoff control for the pressure but would not expect this to be the primary issue.

2. PROBLEM FORMULATION

2.1. *Equations of Motion*

The two-dimensional compressible Navier–Stokes equations using the time-derivative preconditioning procedure can be written in the vector form

$$\Gamma \frac{\partial Q}{\partial t} + \frac{\partial E}{\partial x} + \frac{\partial F}{\partial y} = H + L(Q_v), \tag{1}$$

where Γ is the preconditioning matrix and will take on various forms depending on the preconditioning chosen. Here, we present the equations in Cartesian coordinates, although all computations have been prepared in generalized coordinates. When Γ is the identity matrix, we recover the standard (non-preconditioned) equations. Additional vectors in Eq. (1) are:

$$\begin{aligned} Q &= (\rho, \rho u, \rho v, e)^{\mathrm{T}} \\ E &= (\rho u, \rho u^2 + p, \rho uv, (e+p)u)^{\mathrm{T}} \\ F &= (\rho v, \rho uv, \rho v^2 + p, (e+p)v)^{\mathrm{T}} \\ H &= (0, 0, -\rho g, -\rho g v)^{\mathrm{T}} \\ Q_v &= (p, u, v, T)^{\mathrm{T}}. \end{aligned} \tag{2}$$

In these expressions, the dependent vector Q and the inviscid flux vectors E and F take their standard form, while H is the source vector, which contains a gravitational body force. The vector Q_v represents the "viscous" variables that appear in the diffusion operators. The use of Q_v instead of Q in the diffusion terms simplifies their structure, thus reducing the computational complexity.

All the variables in Eq. (2) are defined by standard notation including density ρ, velocity components u and v, pressure p, temperature T, and total energy per unit volume e. The coordinate system is oriented so that the gravitational body force is in the negative y-direction. The gravitational term $\rho g v$ is the work done by the gravity force. The pressure can be obtained from the equation of state for a perfect gas.

$$p = (\gamma - 1)\left(e - \frac{\rho}{2}(u^2 + v^2)\right), \tag{3}$$

where γ is the ratio of specific heats.

The differential operator for the viscous terms is denoted by L which is defined as

$$\begin{aligned} L = &\frac{\partial}{\partial x} R_{xx} \frac{\partial}{\partial x} + \frac{\partial}{\partial x} R_{xy} \frac{\partial}{\partial y} \\ &+ \frac{\partial}{\partial y} R_{yx} \frac{\partial}{\partial x} + \frac{\partial}{\partial y} R_{yy} \frac{\partial}{\partial y}. \end{aligned} \tag{4}$$

The matrices R_{xx}, R_{xy}, R_{yx}, and R_{yy} are diffusion coefficient matrices that include the viscosity μ and the thermal conductivity k:

$$R_{xx} = \begin{pmatrix} 0 & 0 & 0 & 0 \\ 0 & \frac{4}{3}\mu & 0 & 0 \\ 0 & 0 & \mu & 0 \\ 0 & \frac{4}{3}\mu u & \mu v & k \end{pmatrix}, \quad R_{xy} = \begin{pmatrix} 0 & 0 & 0 & 0 \\ 0 & 0 & -\frac{2}{3}\mu & 0 \\ 0 & \mu & 0 & 0 \\ 0 & \mu v & -\frac{2}{3}\mu u & 0 \end{pmatrix}$$

$$R_{yx} = \begin{pmatrix} 0 & 0 & 0 & 0 \\ 0 & 0 & \mu & 0 \\ 0 & -\frac{2}{3}\mu & 0 & 0 \\ 0 & -\frac{2}{3}\mu v & \mu u & 0 \end{pmatrix}, \quad R_{yy} = \begin{pmatrix} 0 & 0 & 0 & 0 \\ 0 & \mu & 0 & 0 \\ 0 & 0 & \frac{4}{3}\mu & 0 \\ 0 & \mu u & \frac{4}{3}\mu v & k \end{pmatrix} \tag{5}$$

In these expressions, Stoke's hypothesis is used for the second coefficient of viscosity ($\lambda = -\frac{2}{3}\mu$).

2.2. *Development of Preconditioning Procedure*

The preconditioning matrix that was chosen in our earlier work [8, 10] takes the form:

$$\Gamma=\begin{pmatrix} 1 & 0 & 0 & 0 \\ 0 & 1 & 0 & 0 \\ 0 & 0 & 1 & 0 \\ \dfrac{u^2+v^2}{2}(M^{-2}-1) & u(1-M^{-2}) & v(1-M^{-2}) & M^{-2} \end{pmatrix}, \tag{6}$$

where M is Mach number. As can be seen by inspection, this preconditioning leaves the continuity and momentum equations in their traditional form, but modifies the energy equation such that time derivatives of ρ, ρu, and ρv are added. Both stability analyses and various numerical experiments show that this preconditioning matrix is effective for a wide variety of inviscid low Mach number calculations [8, 10]. Classical linear stability analyses of the full Navier–Stokes equations in vector form, however, as well as numerical experiments, show that it is unstable at low Reynolds numbers. Detailed analysis [9] indicates that this instability depends primarily upon the Prandtl number. In the presence of approximate factorization, the Euler implicit scheme is highly unstable for Peclet numbers below 500 and in the absence of approximate factorization, the scheme retains a weak instability. To demonstrate this, the magnitudes of the maximum eigenvalues of the amplification matrix for the Navier–Stokes equations at a Reynolds number of 50 and a Mach number of 10^{-5} are presented in Fig. 1. For the approximately factored equations at a Prandtl number of 0.7, Fig. 1a shows amplification factors are substantially greater than unity at high wave numbers in x and moderate wave numbers in y and at high wave numbers in y and moderate wave numbers in x. In the absence of approximate factorization, the system demonstrates instability at low wave numbers, Fig. 1b, when the Prandtl number of 0.07. This strong dependence of the stability characteristics on the Prandtl number suggests that the modified energy equation may no longer be well posed in the diffusion limit.

A possible insight into the difficulties may be gained by looking at the temperature form of the energy equation. With minor manipulation, we obtain the following temperature form of the energy for the preconditioned system (1) with Eq. (6):

$$\rho C_p\left(\frac{\partial T}{\partial t}+u\frac{\partial T}{\partial x}+v\frac{\partial T}{\partial y}\right) - \left[\frac{(\gamma-1/M^2)}{(\gamma-1)}\frac{\partial p}{\partial t}+u\frac{\partial p}{\partial x}+v\frac{\partial p}{\partial y}\right] = \nabla\cdot(k\nabla T)+\Phi, \tag{7}$$

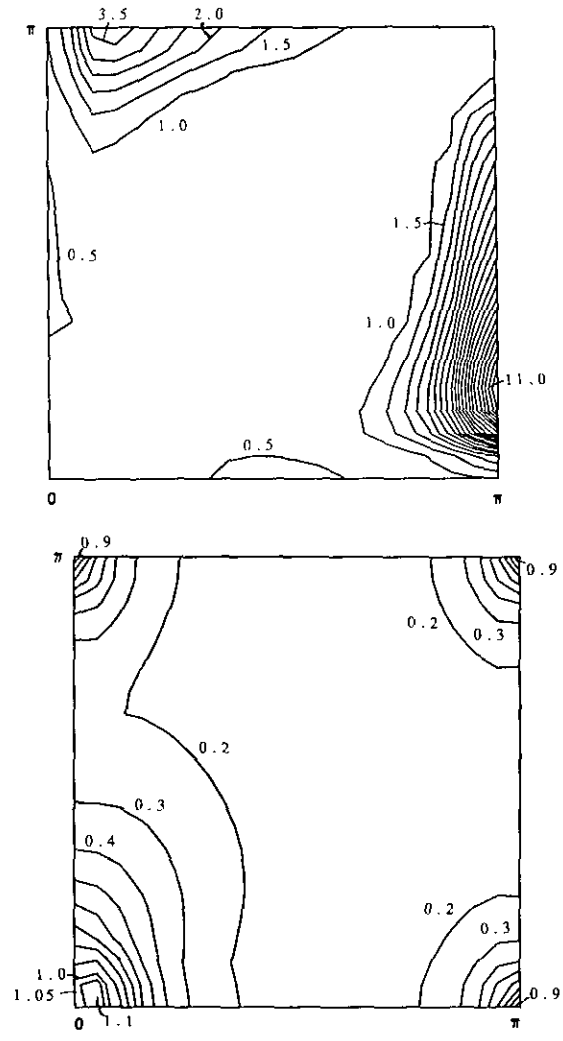

FIG. 1. (a) Stability results for the preconditioning algorithm using Eq. (6) with approximate factorization, $M=10^{-5}$, Re = 50, Pr = 0.7, CFL = 5, $\sigma_\mu=3.09$, $\sigma_k=4.42$. (b) Stability results for the preconditioning algorithm using Eq. (6) without approximate factorization, $M=10^{-5}$, Re = 50, Pr = 0.07, CFL = 5, $\sigma_\mu=3.09$, $\sigma_k=44.2$.

where Φ is the dissipation function defined by

$$\Phi=\mu\left[2\left(\frac{\partial u}{\partial x}\right)^2+2\left(\frac{\partial v}{\partial y}\right)^2 +\left(\frac{\partial v}{\partial x}+\frac{\partial u}{\partial y}\right)^2-\frac{2}{3}\left(\frac{\partial u}{\partial x}+\frac{\partial v}{\partial y}\right)^2\right]. \tag{8}$$

Here every term in Eq. (7), except the time derivative of pressure, retains its traditional form. We can see that a decrease in the Mach number changes the sign of the time derivative of the pressure. This change of sign may not be appropriate for the conduction term and is a probable cause of the instability.

To circumvent this difficulty, a new preconditioning matrix that is effective both in inviscid and viscous calculations is developed in the present paper. The basic idea of the new time-derivative preconditioning procedure is to start with the time derivatives expressed in terms of the "viscous" dependent variables (Q_v) that appear in the diffusion terms. This set of variables is inspired by artificial compressibility methods for incompressible flow [4, 8] as well as low Mach number formulations using perturbation expansions for compressible flow [9, 12] and makes it easier to ensure that there is no time reversal in the viscous terms. In particular, the low Mach number formulation with this set of variables provides unconditionally stable results for both inviscid and viscous calculations. We also note that "viscous" dependent variables (Q_v) are very similar to the (p, u, v, S) variables used by Turkel [4], except entropy is replaced by temperature.

To simplify the algebra, first we transform the conservative form of Eq. (1) to the non-conservative form. We define the non-conservative vector as

$$\tilde{Q} = (\rho, u, v, p)^{\mathrm{T}}, \tag{9}$$

where the tilde represents the non-conservative variable. We then premultiply Eq. (1) by the Jacobian $P^{-1} = \partial\tilde{Q}/\partial Q$ to obtain

$$\frac{\partial\tilde{Q}}{\partial t} + P^{-1}\left(\frac{\partial E}{\partial x} + \frac{\partial F}{\partial y}\right) = P^{-1}(H + L(Q_v)). \tag{10}$$

Here the preconditioning matrix is dropped for the time being.

One convenient method for obtaining a new preconditioning matrix, as well as for transforming the (ρ, u, v, p) system to the (p, u, v, T) system, is as follows. First we subtract the continuity equation from the energy equation. This introduces the temperature form of the time derivative into the energy equation ($\partial\rho/\partial t$ in the continuity equation is replaced by $\partial T/\partial t$ by means of the perfect gas law.) This temperature form of the time derivative appears well-suited to the heat diffusion term.

The vector form of this step is obtained by premultiplying Eq. (10) by a sparse matrix K_1,

$$K_1\frac{\partial\tilde{Q}}{\partial t} + K_1P^{-1}\left(\frac{\partial E}{\partial x} + \frac{\partial F}{\partial y}\right) = K_1P^{-1}(H + L(Q_v)), \tag{11}$$

where

$$K_1 = \mathrm{Diag}(1, \rho, \rho, 1), \text{ with nonzero element } (4, 1) = -\gamma RT. \tag{12}$$

We then convert the dependent vector $\tilde{Q}$ to Q_v by using the chain rule,

$$K_1K_2\frac{\partial Q_v}{\partial t} + K_1P^{-1}\left(\frac{\partial E}{\partial x} + \frac{\partial F}{\partial y}\right) = K_1P^{-1}(H + L(Q_v)), \tag{13}$$

where K_2 is defined as the Jacobian, $K_2 = \partial\tilde{Q}/\partial Q_v$. Now we precondition Eq. (13) by premultiplying the time derivative term by $\Gamma_vK_2^{-1}K_1^{-1}$ to obtain

$$\Gamma_v\frac{\partial Q_v}{\partial t} + K_1P^{-1}\left(\frac{\partial E}{\partial x} + \frac{\partial F}{\partial y}\right) = K_1P^{-1}(H + L(Q_v)), \tag{14}$$

where the preconditioning matrix Γ_v is defined as

$$\Gamma_v = \begin{pmatrix} \dfrac{1}{\beta M^2} & 0 & 0 & 0 \\ 0 & \rho & 0 & 0 \\ 0 & 0 & \rho & 0 \\ (1-\gamma)\delta & 0 & 0 & \gamma\rho R \end{pmatrix} \tag{15}$$

and where βM^2 is a scaling parameter (M is Mach number) and δ is an arbitrary constant, the proper choice of which is discussed later. This preconditioning matrix Γ_v introduces the artificial compressibility form of the continuity equation and modifies the energy equation to its classical temperature form, while keeping the momentum equations in their standard form.

These preconditioned equations are nearly identical to the perturbation equations used extensively [9, 12, 14–16]. The individual equations are

$$\begin{aligned} &\frac{1}{\beta M^2}\frac{\partial p}{\partial t} + \frac{\partial(\rho u)}{\partial x} + \frac{\partial(\rho v)}{\partial y} = 0 \\ &\rho\left(\frac{\partial u}{\partial t} + u\frac{\partial u}{\partial x} + v\frac{\partial u}{\partial y}\right) + \frac{\partial p}{\partial x} = \rho(\text{V.T.}) \\ &\rho\left(\frac{\partial v}{\partial t} + u\frac{\partial v}{\partial x} + v\frac{\partial v}{\partial y}\right) + \frac{\partial p}{\partial y} = \rho(\text{V.T.}) \\ &\rho C_p\left(\frac{\partial T}{\partial t} + u\frac{\partial T}{\partial x} + v\frac{\partial T}{\partial y}\right) = \delta\frac{\partial p}{\partial t} + u\frac{\partial p}{\partial x} + v\frac{\partial p}{\partial y} \\ &\qquad + \nabla\cdot(k\nabla T) + \Phi. \end{aligned} \tag{16}$$

The term V.T. represents the appropriate viscous term as given in Eq. (5) and Φ is the dissipation function given above. We note that in the energy equation, δ appears as a coefficient of the time derivative of pressure. From inspection of the equation, two convenient choices of δ may be 0 or 1.

When $\delta = 0$, the time derivative of pressure drops out, and when $\delta = 1$, a standard energy equation can be retained. With either choice of δ, the momentum and the energy equations now appear to be well-suited for viscous effects, since they are all of the form

$$\frac{\partial \phi}{\partial t} + V \cdot \nabla \phi = \alpha \nabla^2 \phi, \tag{17}$$

where ϕ represents u, v, and T, respectively, and α is the appropriate diffusivity.

The corresponding time-derivative preconditioned system for the conservative form of the equations is readily found by premultiplying Eq. (14) by PK_1^{-1} to obtain

$$\bar{\Gamma} \frac{\partial Q_v}{\partial t} + \frac{\partial E}{\partial x} + \frac{\partial F}{\partial y} = H + L(Q_v). \tag{18}$$

Here, $\bar{\Gamma}$, defined as $\bar{\Gamma} = PK_1^{-1}\Gamma_v$, is

$$\bar{\Gamma} = \begin{pmatrix} \dfrac{1}{\beta M^2} & 0 & 0 & 0 \\ \dfrac{u}{\beta M^2} & \rho & 0 & 0 \\ \dfrac{v}{\beta M^2} & 0 & \rho & 0 \\ \dfrac{(e+p)}{\rho \beta M^2} - \delta & \rho u & \rho v & \dfrac{\gamma \rho R}{\gamma - 1} \end{pmatrix}. \tag{19}$$

The eigenvalues of the preconditioned system of Eqs. (18) are

$$\lambda(\bar{\Gamma}^{-1} A_v) = \left(u, u, \frac{u(1 + \beta M^2 \omega / \gamma RT) \pm c'}{2} \right), \tag{20}$$

where $A_v = \partial E / \partial Q_v$ and $\omega = \gamma - (\gamma - 1)\delta$. The pseudo-acoustic speed c' is defined as

$$c'^2 = u^2 \left(1 + \frac{\beta M^2 \omega}{\gamma RT} \right)^2 + 4 \beta M^2 \left(1 - \frac{u^2}{\gamma RT} \right). \tag{21}$$

In the present study, $\delta = 1$ (thus, $\omega = 1$) is used and this value with a proper choice of β gives identical eigenvalues to those obtained from the preconditioning matrix of Eq. (6). Representative computations with $\delta = 0$ give convergence rates that are almost identical to those with $\delta = 1$.

In order to obtain well-conditioned eigenvalues for the inviscid case, we choose the scaling parameter $\beta = k\gamma RT$, where k is a parameter to be determined later. For values of k of order unity, this choice of β allows the pseudo-acoustic wave speed c' to be the same order as the particle velocity u and ensures that three eigenvalues are always positive, while one is negative for subsonic flow. As Mach number approaches unity, the eigenvalues return to the physically proper values $(u, u, u + c, u - c)$.

The solutions given herein are obtained from the form of equations given in Eq. (18) with the preconditioning matrix, Eq. (19). For completeness we transform the matrix in Eq. (19) to a form that is analogous to Eq. (6) so that direct comparison can be made. This is accomplished by multiplying Eq. (19) by the Jacobian $\partial Q_v / \partial Q$. The result is

$$\Gamma = \begin{pmatrix} \dfrac{(\gamma-1)(u^2+v^2)}{2\beta M^2} & \dfrac{(1-\gamma)u}{\beta M^2} & \dfrac{(1-\gamma)v}{\beta M^2} & \dfrac{(\gamma-1)}{\beta M^2} \\ u\left[\dfrac{(\gamma-1)(u^2+v^2)}{2\beta M^2} - 1\right] & 1 + \dfrac{(1-\gamma)u^2}{\beta M^2} & \dfrac{(1-\gamma)uv}{\beta M^2} & \dfrac{(\gamma-1)u}{\beta M^2} \\ v\left[\dfrac{(\gamma-1)(u^2+v^2)}{2\beta M^2} - 1\right] & \dfrac{(1-\gamma)uv}{\beta M^2} & 1 + \dfrac{(1-\gamma)v^2}{\beta M^2} & \dfrac{(\gamma-1)v}{\beta M^2} \\ \dfrac{(\gamma-1)(u^2+v^2)}{2}(\theta+2) - \dfrac{\gamma e}{\rho} & u(1-\gamma)(\theta+1) & v(1-\gamma)(\theta+1) & \theta(\gamma-1)+\gamma \end{pmatrix} \tag{22}$$

where $\theta = (e + p)/\rho\beta M^2 - \delta$. Comparison of the new "viscous" preconditioning matrix (Eq. 22) and the "inviscid" preconditioning matrix (Eq. (6)) shows that the two matrices are completely different. The "inviscid" preconditioning matrix is much simpler than the "viscous" one, and this complexity is avoided by using the "viscous" dependent variables (Q_v). As mentioned before, in the non-conservative form, the "viscous" preconditioning matrix essentially modifies the continuity equation, while the "inviscid" preconditioning matrix modifies the energy equation. In the transformation to conservative form, the modified continuity equation is combined with the momentum and the energy equations. It is this step that brings about complexity in the "viscous" preconditioning matrix, Eq. (22).

One difficulty associated with the above preconditioning system is that the $1/M^2$ term in the preconditioning matrix becomes singular in regions where Mach number approaches zero (e.g., stagnation points). To circumvent this difficulty, we modify the M^2 term in the preconditioning matrix by replacing M^2 by M_r^2 (where, M_r is a reference Mach number). The value of M_r is controlled

according to flow conditions. For subsonic flow where $M<\varepsilon$ we use $M_r=\varepsilon$, while for supersonic flow where preconditioning is not necessary, we fix M_r as unity to retain the standard eigenvalues. In between the Mach number range, $M_r=M$ is used. The above eigenvalue control can be written as

$$M_r^2=\begin{cases}\varepsilon^2, & \text{if } M<\varepsilon\\ M^2, & \text{if } \varepsilon<M<1\\ 1, & \text{if } M>1.\end{cases} \tag{23}$$

This eigenvalue control is continuous in terms of Mach number and makes the preconditioned system of equations well-behaved in both subsonic and supersonic flow, thus ensuring enhancement of convergence rates. In the present study, ε is typically taken as 10^{-5} in the vicinity of stagnation points.

2.3. *Convergence Control at Low Reynolds Numbers*

Linear stability analyses of Eq. (18) show that the new preconditioning matrix (Eq. (19)) provides appropriate stability for all Reynolds and Peclet numbers. This new preconditioning matrix appears to be at least as good as the original preconditioning for inviscid flow as shown in Fig. 2. Both the previous preconditioning, Eq. (6), and the present one, Eq. (19), have identical stability characteristics. The present preconditioning matrix is, however, a dramatic improvement over the original one for viscous flows (compare Fig. 3 and Fig. 1). At low Reynolds numbers (below $\mathrm{Re}=50$), however, stability characteristics show that amplification factors approach unity, suggesting slow convergence rates (see Fig. 4a). The reason for this behavior can be understood by considering the viscous time step parameter (hereinafter referred to as the von Neumann number) $\sigma=\mu\,\Delta t/\rho\,\Delta x^2$, which becomes important at low Reynolds numbers. Control of the CFL number alone at low Reynolds number makes the von Neumann number so large that the approximate factorization error in the diffusive terms slows convergence. For efficient convergence, we should control both the CFL number and the von Neumann number simultaneously.

The simultaneous control of the CFL number and the von Neumann number is obtained by choosing the scaling parameter k in the definition of β. The parameter k is chosen as unity ($\beta=\gamma RT$) to obtain well-conditioned eigenvalues for the inviscid terms. In low Reynolds number flow, however, we use this parameter to specify both CFL and von Neumann numbers. In the inviscid limit, we choose the time step by an appropriate CFL number,

$$\mathrm{CFL}=\frac{(u(1+kM_r^2)+c')\,\Delta t}{2\Delta x}, \tag{24}$$

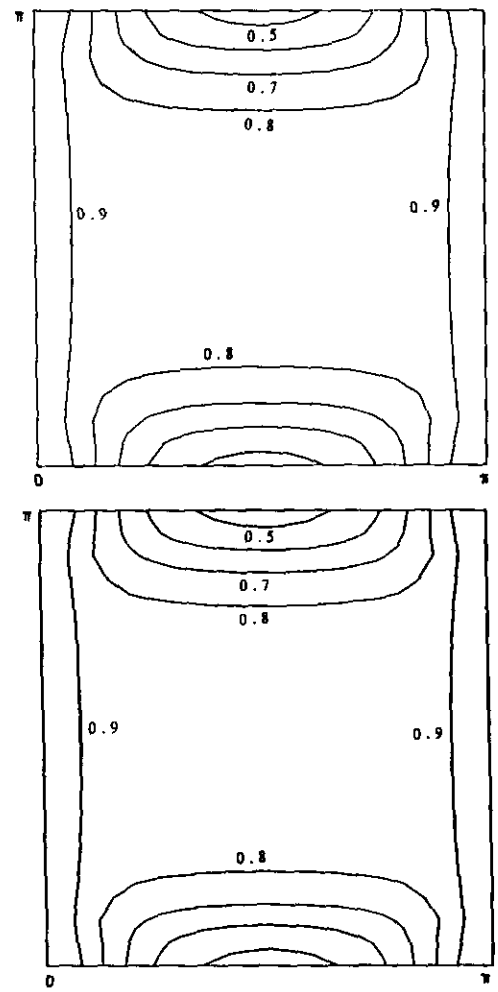

FIG. 2. (a) Stability results for the preconditioning algorithm using Eq. (6) with approximate factorization (inviscid flow), $M=10^{-5}$, $\mathrm{CFL}=5$. (b) Stability results for the preconditioning algorithm using Eq. (19) with approximate factorization (inviscid flow), $M=10^{-5}$, $\mathrm{CFL}=5$.

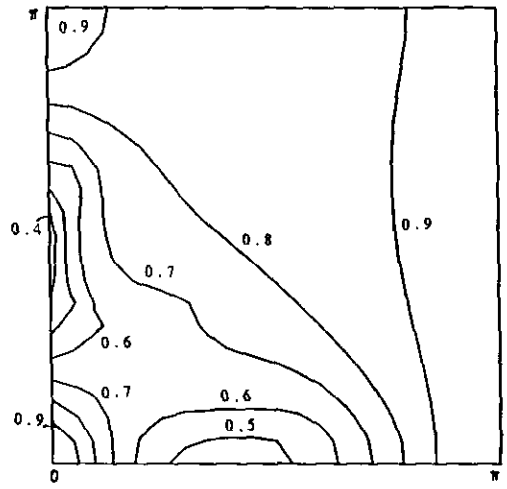

FIG. 3. Stability results for the preconditioning algorithm using Eq. (19) with approximate factorization, $M=10^{-5}$, $\mathrm{Re}=50$, $\mathrm{Pr}=0.7$, $\mathrm{CFL}=5$, $\sigma_\mu=3.09$, $\sigma_k=4.42$.

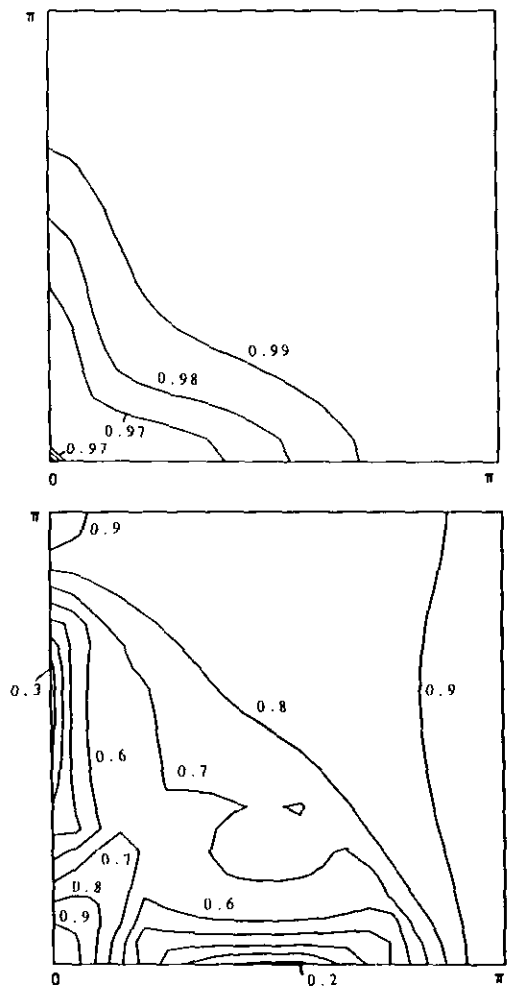

FIG. 4. (a) Stability results for the preconditioning algorithm using Eq. (19) with approximate factorization, $M = 10^{-5}$, $\mathrm{Re} = 1$, $\mathrm{Pr} = 0.7$, $\mathrm{CFL} = 5$, $\sigma_\mu = 154.5$, $\sigma_k = 220.73$. (b) Stability results for the preconditioning algorithm using Eq. (19) with approximate factorization, $M = 10^{-5}$, $\mathrm{Re} = 1$, $\mathrm{Pr} = 0.7$, $\mathrm{CFL} = 5$, $\sigma_\mu = 3.0$, $\sigma_k = 4.3$, $k = 6860$.

while in the viscous limit, the appropriate viscous time step parameter is the von Neumann number. By solving Eq. (24) and the above von Neumann number definition for k, we find

$$k = \frac{\alpha(\alpha - 1)}{M_r^2(\alpha - 1 + \gamma RT/u^2)}, \tag{25}$$

where α is $\mathrm{CFL}/\sigma\ \mathrm{Re}_{\Delta x}$ and $\mathrm{Re}_{\Delta x}$ is the cell Reynolds number ($= \rho u\, \Delta x/\mu$). Now, by setting the CFL number and the von Neumann number to order unity and computing other variables from given conditions, we can obtain the scaling factor k. In general, for a wide range of Reynolds number, the parameter k can be expressed by

$$k = \mathrm{Max}\left[1, \frac{\alpha(\alpha - 1)}{M_r^2(\alpha - 1 + \gamma RT/u^2)}\right]. \tag{26}$$

Figure 4b shows the stability characteristics for the $\mathrm{Re} = 1$ case when the preconditioning of Eq. (19) is used along with the value of k given by Eq. (26). Comparison with Fig. 4a shows the improvement obtained. In the present paper, calculations for low Reynolds number flow employ a spatially varying k so that a constant von Neumann number can be maintained over the flow domain.

2.4. *Roundoff Error Control*

Another difficulty with low Mach number computations is the increase in machine roundoff errors with decreasing Mach number. It was shown [9] that roundoff error begins to dominate below $M = 10^{-3}$ and it increases proportional to M^2. The cause of this roundoff error arises from the calculation of pressure gradients. This problem can be easily circumvented by employing a gauge pressure,

$$p = \bar{p} + p', \tag{27}$$

where $\bar{p}$ is an arbitrary constant. We then redefine Q_v, E, and F as follows:

$$\begin{aligned} Q_v &= (p', u, v, T)^{\mathrm{T}} \\ E &= (\rho u, \rho u^2 + p', \rho uv, (e + p)u)^{\mathrm{T}} \\ F &= (\rho v, \rho uv, \rho v^2 + p', (e + p)v)^{\mathrm{T}}. \end{aligned} \tag{28}$$

The perfect gas relation, Eq. (3) remains unchanged.

3. NUMERICAL SOLUTION PROCEDURE

Appropriate preconditioning enhances convergence of either explicit or implicit algorithms [10]. Here, the numerical solution of Eq. (18) with Eq. (28) is obtained by using an Euler implicit discretization in time along with central differencing in space. For the efficient solution of the resulting matrix, we use an approximate factorization such as the Douglas–Gunn procedure [21, 22]. This leads to

$$\begin{aligned} &\left[I + \Delta t\, S^{-1}\left(\frac{\partial A}{\partial x} - \frac{\partial}{\partial x} R_{xx} \frac{\partial}{\partial x}\right)\right] \\ &\quad \times \left[I + \Delta t\, S^{-1}\left(\frac{\partial B}{\partial y} - \frac{\partial}{\partial y} R_{yy} \frac{\partial}{\partial y}\right)\right] \Delta Q_v \\ &\quad = -\Delta t\, S^{-1} R, \end{aligned} \tag{29}$$

where R is the residual of the steady state version of Eq. (18),

$$R = \frac{\partial E}{\partial x} + \frac{\partial F}{\partial y} - L(Q_v) - H. \tag{30}$$

Here A, B, and D are Jacobians of the vectors E, F, and H and the matrix $S=\bar{\Gamma}-\Delta t\, D$. The solution of Eq. (29) requires a standard block tridiagonal matrix inversion procedure. This formulation differs from the traditional approximately factored algorithm only in the calculation of the preconditioning matrix, and hence additional computational cost is negligible. In some calculations, a fourth-order artificial dissipation is added in an explicit manner.

An important aspect of the preconditioning scheme given here is that its effects are present only on the left-hand side of the discretized equations (Eq. (29)) when they are written in delta form. Consequently, the preconditioning has no effect on the steady solution. Comparison of solutions converged to machine accuracy using preconditioning and those obtained without preconditioning verify this. The residuals of the preconditioned equation identically satisfy the nonpreconditioned operator (to machine precision) and conversely. Note that these comments are made for the case of central difference operators only. It is possible that preconditioning does impact the steady solution when flux difference split operators that depend on the preconditioning matrix are used. The roundoff errors in pressure noted earlier are because of the low Mach numbers, not because of preconditioning.

4. BOUNDARY CONDITIONS

The proper choice of boundary conditions is extremely important to any numerical algorithm. In the present study, the method of characteristics-based boundary conditions [12] are used at inflow and outflow boundaries. It is imperative to incorporate the preconditioning matrix in this procedure to reflect the character of pseudo-acoustic waves near the boundaries. To apply the method of characteristics procedure, we first premultiply Eq. (29) by the modal matrix M^{-1}, containing the left eigenvector of the Jacobian $\Gamma^{-1}A$ (or $\Gamma^{-1}B$) at a constant x (or y) boundary. We then multiply the result by a selection matrix L that selects those characteristic equations that represent outgoing information at the boundaries. The approximate set of equations in the method of characteristics procedure can be written in the form

$$LM^{-1}\left[I+\Delta t\, S^{-1}\frac{\partial A}{\partial x}\right]\times\left[I+\Delta t\, S^{-1}\left(\frac{\partial B}{\partial y}-\frac{\partial}{\partial y}R_{yv}\frac{\partial}{\partial y}\right)\right]\Delta Q_v = -\Delta t\, LM^{-1}S^{-1}R. \tag{31}$$

Note that this method of characteristics procedure is based upon the artificial characteristics of the preconditioned system, because the physical characteristics have been removed.

In Eq. (31), the selection matrix L has different forms, depending on the boundaries of interest. For inflow boundaries, where the flow is subsonic, L becomes $L=\mathrm{Diag}(0, 0, 0, 1)$, where the non-zero entry selects the outgoing characteristic equation $(u-c')$, while the zero entries require that physically meaningful boundary conditions be specified. For the present study, stagnation pressure, stagnation temperature, and flow angle (v/u) are fixed. The outflow boundary conditions are also obtained in a similar way. When flow is subsonic, a selection matrix is $L=\mathrm{Diag}(1, 1, 1, 0)$ and a constant static pressure is imposed. For supersonic flow, the selection matrix L becomes the identity matrix and no boundary condition is needed.

The boundary conditions imposed on the solid surface are the no-slip condition and a condition on the normal pressure gradient obtained from the normal momentum equation. In addition, either a specified wall temperature or an adiabatic wall condition is specified, depending on the problem. The axis of symmetry is treated as a regular field point using symmetry conditions in lieu of boundary conditions. In all calculations, the above boundary conditions are treated implicitly.

5. RESULTS

Representative results are given for various problems including flow past an isolated airfoil, flow past a circular cylinder, flow through a strongly converging nozzle, and flow in a driven cavity and in a thermally driven cavity. Several additional problems have also been successfully computed with the method but are not presented for reasons of space. In all cases it was demonstrated that the preconditioning changed only the rate of convergence, not the final results. Consequently, we focus on comparing the convergence rates of the various problems with and without preconditioning, although we also include comparisons with previous computations to verify the accuracy of our solutions. The savings realized with preconditioning range from a factor of two to several orders of magnitude.

5.1. *Flow Past an Isolated Airfoil*

The first test problem considers inviscid and viscous flow past a NACA0012 airfoil at zero angle of attack. A C-type grid (56×31) is used and the outer boundary is located five chord lengths away from the wall. Since the flowfield is symmetric, only the half domain is considered. At the wall, a slip boundary condition is used for inviscid flows, while no-slip, constant wall temperature, and zero normal pressure gradient are specified for viscous flows. At the outer boundary for both inviscid and viscous cases, the stagnation pressure, stagnation temperature, and inflow angle are specified for the inflow region, while constant pressure is

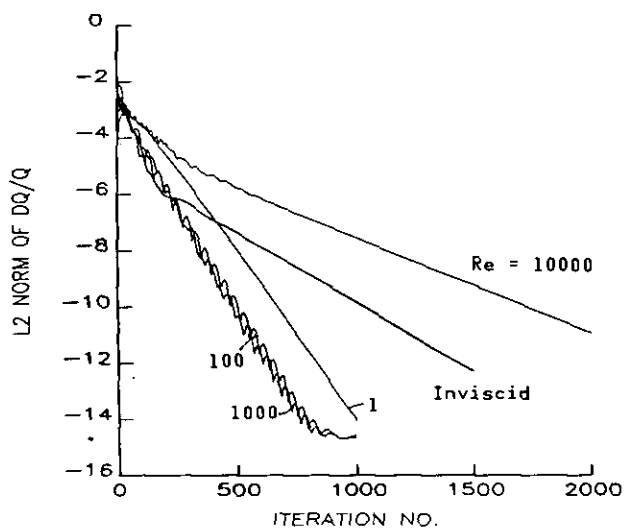

FIG. 5. Convergence rates using preconditioning method for flow past a NACA0012 airfoil for inviscid and viscous cases, $M = 10^{-4}$. For Re = 1, 100, 1000 (CFL = 6, $\sigma = 3$, variable k), for Re = 10,000 (CFL = 3, $k = 1$), for inviscid case (CFL = 6, $k = 1$).

specified at the downstream end. The remaining conditions come from the method of characteristics. The outer free stream Mach number is 10^{-4}, and the viscosity is changed to vary the Reynolds number. This problem could, of course, be computed with the incompressible equations, but the compressible equations are used to demonstrate the capabilities of the preconditioning scheme.

Figure 5 shows the convergence characteristics using the preconditioning method for a wide range of flow conditions from inviscid flow (Re = ∞) to very viscous flow (Re = 1). For all cases, a stretched grid, chosen to provide boundary layer resolution at Re = 10,000 was used. Consequently, the demonstrated convergence rates are the result of changes in Reynolds number, not grid size. The convergence of the inviscid case indicates a rate of convergence of one order of magnitude per 200 iterations. Convergence of the standard algorithm, without preconditioning, was extremely slow, requiring some 100,000 iterations for one order of convergence. Thus preconditioning accelerated convergence in this case by two or three orders of magnitude. For viscous cases of Reynolds numbers of 1, 100, and 1000, it can be seen that the convergence rate is faster by a factor of two than that of the inviscid case. This convergence enhancement at viscous conditions may be because physical diffusion serves to dissipate the errors in the solution more rapidly. At Re = 10,000, however, a slight slowdown in convergence can be noted because the optimum CFL was somewhat lower than for the inviscid and the low Reynolds number cases. In all cases, however, it is clear that the preconditioning procedure enables convergence at these very incompressible flow speeds with efficiencies that are equal to those normally observed in subsonic flows.

The corresponding converged velocity results for the three viscous cases are shown in Fig. 6. The top figures show the full domain solutions, while the bottom figures show the magnified results around the airfoil. At Reynolds number 1, the flow is nearly symmetric around the airfoil, approaching Stokes flow. As Reynolds number increases, the boundary layer gets thinner and at Reynolds number of 10,000, separation is observed at 80% chord. No separation is observed in the other two cases. The solution accuracy was verified by comparing pressure coefficient with incompressible panel method results for the inviscid case. As validations for solutions of several other cases are given below, this comparison is not presented for reasons of space.

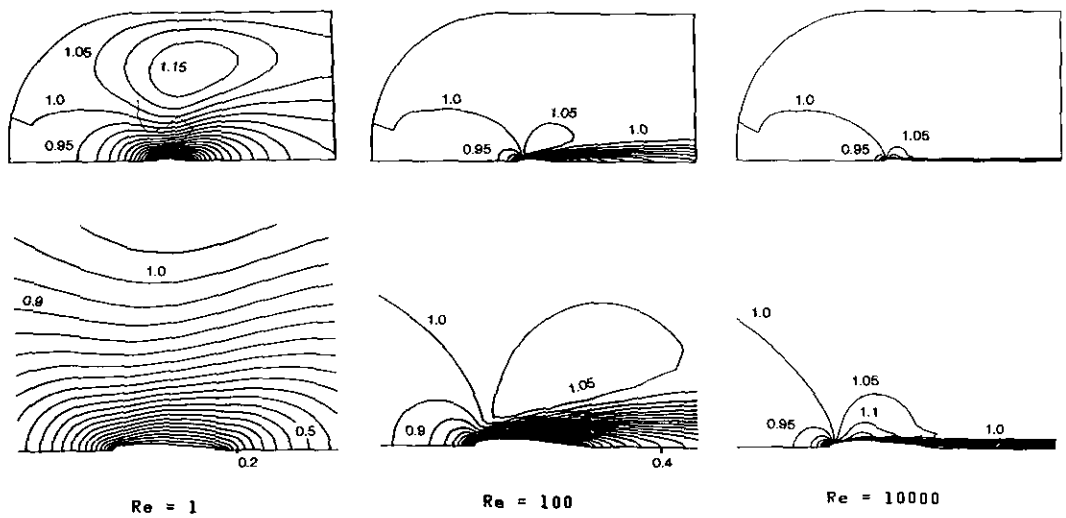

FIG. 6. Velocity (u/u_r) contour plots for viscous flow past a NACA0012 airfoil for Reynolds numbers of 1, 100, and 10,000.

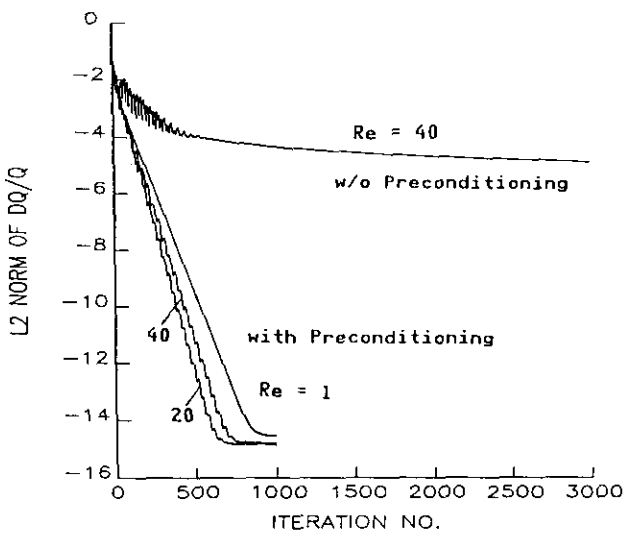

FIG. 7. Convergence rates with and without preconditioning method for flow past a circular cylinder for Re = 1, 20, and 40, $M = 10^{-5}$. For Re = 1, 20, 40 with preconditioning (CFL = 6, $\sigma = 3$, variable k), for Re = 40 without preconditioning (CFL = 6).

5.2. *Flow Past a Circular Cylinder*

The second problem considers viscous flow past a circular cylinder. For this problem, it is known that the flow is steady below Re = 40 and above that value, becomes unsteady with vortex shedding travelling downstream. An O-type grid (98×60) is used and a full (360°) computational domain is employed. The outer boundary is located 20 diameters away from the cylinder and the outer free stream Mach number is about 10^{-5}. The boundary conditions used for the present calculations are identical to those used in the computation of flow past an airfoil.

Convergence characteristics for this problem are shown in Fig. 7 for Reynolds numbers of 40, 20, and 1. At a Reynolds number of 20, the preconditioned system requires about 50 iterations to reduce the L_2 norm of $\Delta Q/Q$ by one order of magnitude. Similar convergence rates can be noted for the other Reynolds number cases and convergence is essentially independent of Reynolds number for these three cases. The convergence of the standard algorithm (without preconditioning) is again very slow, requiring about 5000 iterations for one order of convergence.

Computational results for velocity are shown in the top half of Fig. 8. In the velocity contours at a Reynolds number of 1, the flow tends to divide and reunite smoothly, approaching a symmetric pattern fore and aft. At Reynolds numbers of 20 and 40, the flow separates on the downstream side, and steady standing eddies are formed. These eddies are stable and remain attached to the cylinder. Corresponding pressure contours are shown in the bottom half of Fig. 8. In order to verify the accuracy of the numerical solutions, the pressure coefficient on the wall and the wall vorticity distribution are compared with experimental results by Grove *et al.* [23] and numerical solutions by Fornberg [24] in Fig. 9 and Fig. 10, respectively. In both cases, good agreement can be observed.

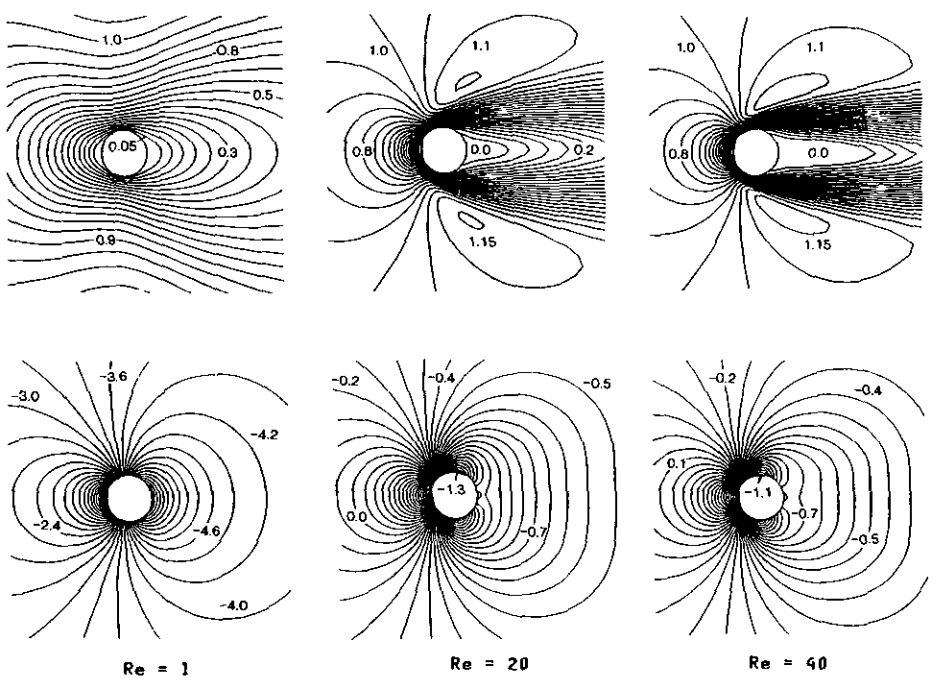

FIG. 8. Velocity (u/u_r) and pressure coefficient (C_p) contour plots for viscous flow past a circular cylinder for Reynolds numbers of 1, 20, and 40. C_p is defined as $C_p = (p - p_0 + 0.5\rho u_r^2)/(0.5\rho u_r^2)$, where p_0 is front stagnation pressure.

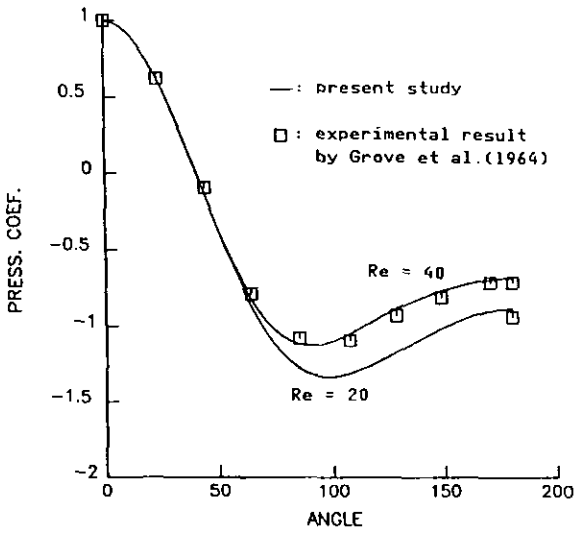

FIG. 9. Comparison of wall pressure coefficient with experimental results by Grove *et al.* [23].

5.3. *Flow through a Strongly Converging Nozzle*

The third test problem concerns the flow through a strongly converging–diverging nozzle. This test problem typifies a high-speed flow with an embedded region of low velocity in which compressibility effects are significant due to the presence of transonic speed flow. Two nozzle geometries are considered for contraction area ratios (AR) of 10 and 200. These nozzle geometries are of interest to us for applications in solar propulsion [1], which requires strongly converging nozzles because of the dilute nature of solar radiation.

Calculations for viscous, choked flow in nozzles with AR = 10 and AR = 200 are made. The converged Mach

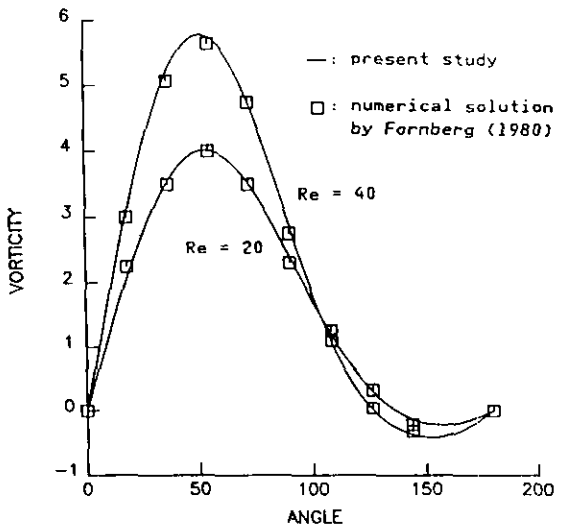

FIG. 10. Comparison of wall vorticity distribution with numerical solutions by Fornberg [24].

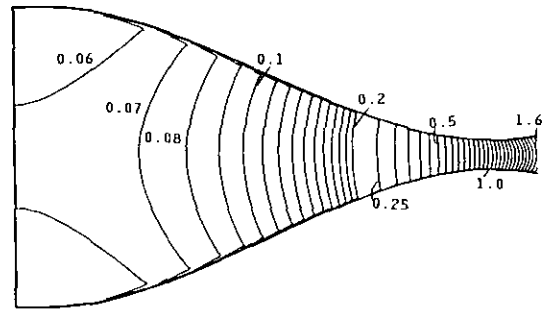

FIG. 11. Mach number contour plot in a strongly converging–diverging nozzle (AR = 10).

number plots and the nozzle geometries are shown in Figs. 11 and 12. A 71×31 grid for AR = 10 and a 100×50 grid for AR = 200 are used with clustering at the wall. In both cases, calculations go through the transonic region and stop in the supersonic region, where supersonic outflow boundary conditions can be specified. The Reynolds number based on the throat diameter is 6×10^6 for AR = 10 and 9×10^5 for AR = 200, respectively. Because of the strong nozzle convergence, the Mach numbers in the upstream sections are about 0.05 (for AR = 10) and 0.002 (for AR = 200), respectively (see Figs. 11 and 12). In Fig. 13, the convergence rate with and without preconditioning is compared. Without preconditioning, it takes 450 steps for AR = 10 and 2100 steps for AR = 200 to reduce one order of magnitude in $\Delta Q/Q$, while with preconditioning it takes 50 steps for AR = 10 and 100 steps for AR = 200. Thus, the preconditioning method enhances convergence rates by a factor of nine for AR = 10 and 20 for AR = 200, respectively.

In view of the convergence speedups noted in Fig. 13, it is

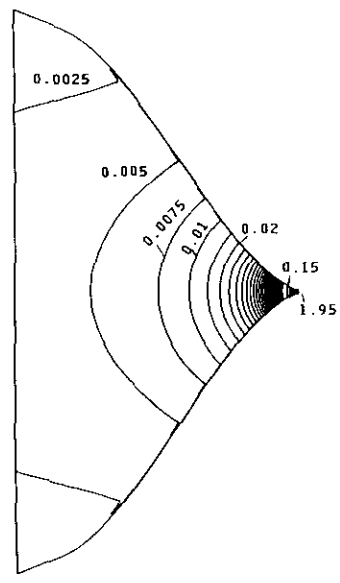

FIG. 12. Mach number contour plot in a strongly converging–diverging nozzle (AR = 200).

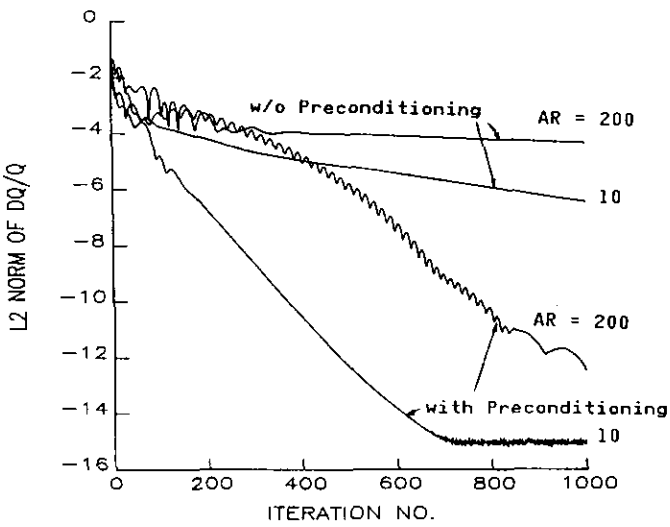

FIG. 13. Convergence rates with and without preconditioning method for viscous flow in a strongly converging-diverging nozzle (AR = 10 and 200). For all cases, CFL = 7, $k = 1$.

important to note that although we have removed the eigenvalue stiffness in the low Mach number region, the equations also become stiff in the transonic flow region where the Mach number goes through unity. This stiffness, however, does not appear to be a problem (as Fig. 13 shows). To investigate this further, we present in Fig. 14 convergence characteristics without preconditioning for the AR = 10 nozzle for several unchoked Mach numbers. The calculations are made for inviscid flow and the nozzle geometry shown in Fig. 11. Throughout the calculations, a 71×31 H-grid is used and the same CFL number is employed. The Mach numbers shown in Fig. 14 indicate the Mach numbers at the throat region. For the $M_t = 0.1$ case, the Mach number variation in the flowfield ranges from $M = 0.01$ in the upstream section to $M = 0.08$ at the nozzle exit, while for the $M_t = 1.0$ case, it ranges from $M = 0.05$ in the upstream section to $M = 1.6$ at the exit.

The figure clearly shows that convergence is slow in all cases, but that it improves (as opposed to slowing down) as the throat Mach number is increased. This improvement is obviously the result of increasing the inlet Mach number from 0.01 to 0.05 and occurs even though the eigenvalues in the throat region are becoming more and more stiff. For example, convergence for a throat Mach number of 0.9 is marginally better than that for 0.8, while convergence for the choked condition ($M_t = 1.0$) is again modestly faster than that for $M_t = 0.9$. There is clearly no adverse effect of eigenvalue stiffness at Mach one as the flow approaches and passes through the sonic speed. Consequently, we conclude that the predominant stiffness in the problem is the one arising from low Mach numbers and that little would be gained by using a generalized (as opposed to a low Mach number) preconditioning for this transonic speed. The reason for this discrepancy is apparently tied to the size of the transonic region in this problem. The number of grid points near the transonic region is small compared to the total flowfield and so it does not have a significant impact on overall convergence.

A similar conclusion concerning small regions of low speed flow can be reached by considering high subsonic (around $M = 0.7$) flow past an airfoil. The stagnation region clearly is stiff in this case, but it is not large enough to cause a slow down in convergence. Consequently, low Mach number preconditioning gives no advantage in such a problem. A second observation concerning generalized preconditioning for stiffness at $M = 1.0$ is that it is not possible to

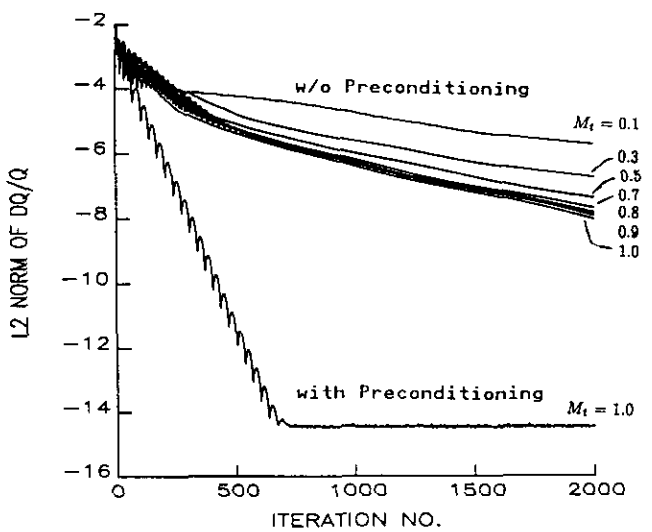

FIG. 14. Convergence rates with and without preconditioning method for inviscid flow in a strongly converging-diverging nozzle (AR = 10). For all cases, CFL = 4, $k = 1$.

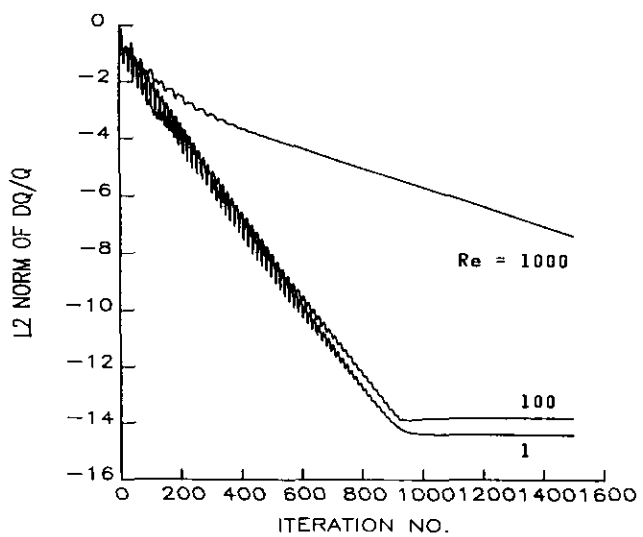

FIG. 15. Convergence rates with preconditioning method for flow in a driven cavity for Re = 1, 100, and 1000. For all cases, CFL = 6, $\sigma = 3$, variable k.

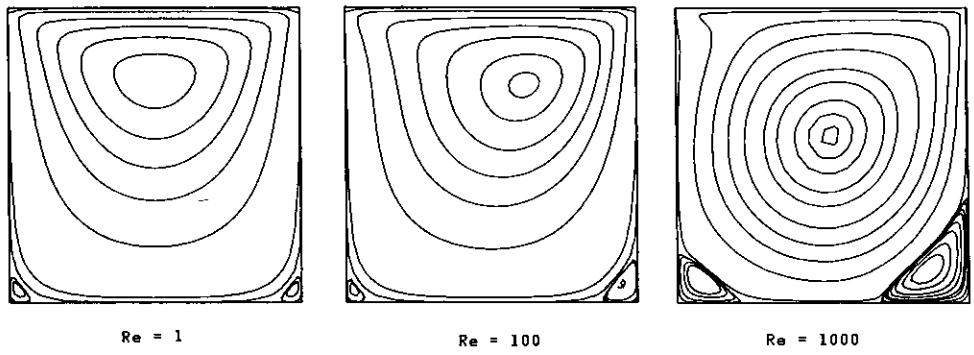

FIG. 16. Streamline contours for flow in a driven cavity for Re = 1, 100, and 1000.

remove the stiffness completely because the eigenvalue is required to pass through zero at $M = 1.0$ [2]. Preconditioning to remove stiffness at $M = 1.0$ can therefore only be used to minimize the region where stiffness has an impact, not to eliminate it. The complexities involved in obtaining a generalized preconditioning method for multidimensional flows, the impossibility of removing the stiffness at the sonic point, and the lack of influence of the sonic region in convergence in typical transonic flows are the reasons we have chosen to concentrate on low Mach number preconditioning.

Finally we note that low Mach number preconditioning enhances convergence of all the unchoked and choked nozzle flow cases in Fig. 14 and results in a convergence speed that is independent of Mach number. Representative results for one such preconditioned case are shown in Fig. 14.

5.4. *Flow in a Driven Cavity*

The fourth test problem considers a flow in a square cavity whose top wall moves with a uniform velocity. This problem served as a benchmark for incompressible Navier–Stokes equations for decades. Three Reynolds number cases 1, 100, and 1000 are considered and a 61×61 grid is employed. A uniform grid is used for Re = 1 and 100, while a stretched grid is used for Re = 1000. Wall boundary conditions are no slip, isothermal condition and zero normal pressure gradient. The Mach number of the moving lid is 4.5×10^{-4}. Figure 15 shows convergence characteristics for the above three Reynolds numbers. At Reynolds numbers of 1 and 100, the preconditioned system requires about 75 iterations for one order of convergence, while at Re = 1000, it requires 300 iterations. The slowdown in convergence at Re = 1000 is mainly due to grid stretching.

Computational results showing streamlines for the above three Reynolds number cases are shown in Fig. 16. The streamline plots show a large primary vortex near the center of the cavity, along with two secondary vortices at the bottom corners. As the Reynolds number increases, a shift of the center of the vortex toward the center of the cavity and a growth of a secondary vortex at the right-hand bottom corner can be noted. The effect of the Reynolds number on

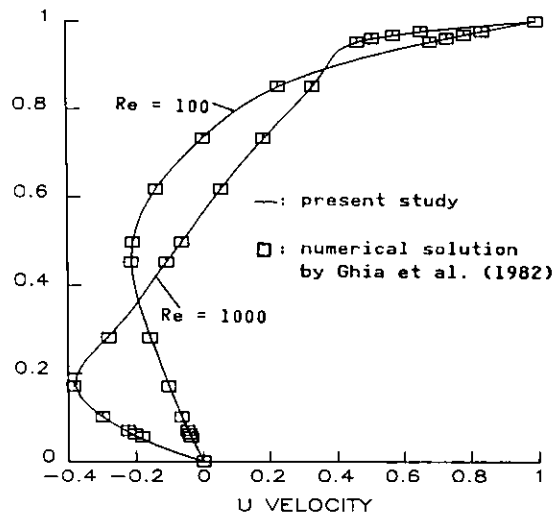

FIG. 17. Comparison of u velocity component at vertical centerline of cavity with numerical solutions by Ghia *et al.* [25].

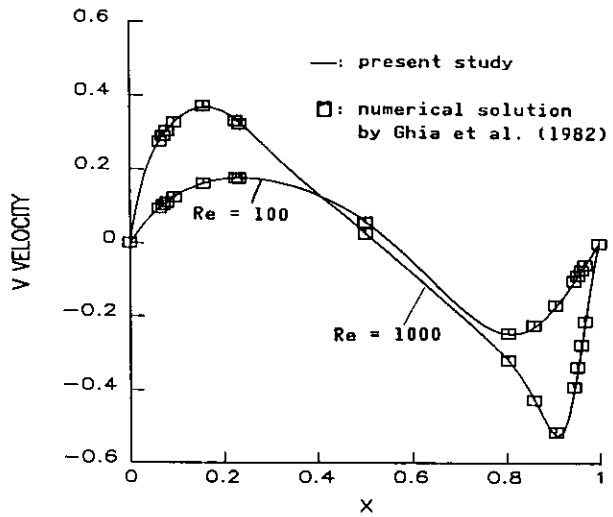

FIG. 18. Comparison of v velocity component at horizontal centerline of cavity with numerical solutions by Ghia *et al.* [25].

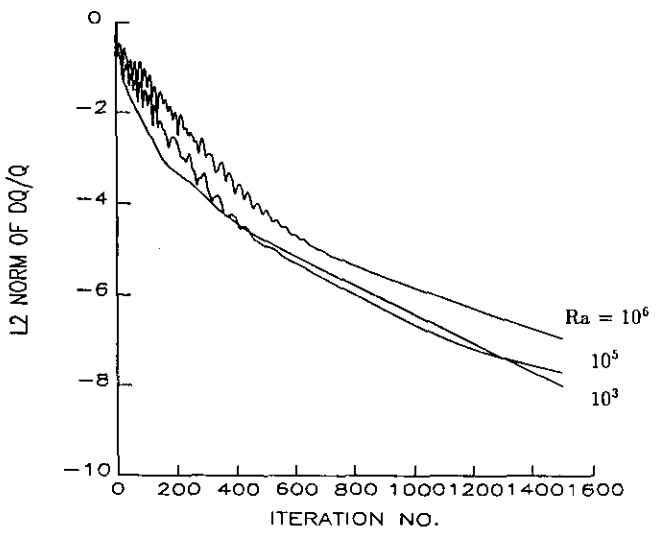

FIG. 19. Convergence rates with preconditioning method for viscous flow in a thermally driven cavity for $Ra = 10^3$, 10^5, and 10^6. For all cases, CFL = 8, $\sigma = 3$, variable k.

the size of the secondary vortex at the left-hand bottom corner is relatively small. To verify the accuracy of numerical solutions, comparison of u and v velocities at the vertical and horizontal centerlines with numerical solutions by Ghia *et al.* [25] is shown in Figs. 17 and 18. Excellent agreement can be observed.

5.5. *Flow in a Thermally Driven Cavity*

The final test problem considers a buoyancy-driven flow in a square enclosure. The configuration consists of two insulated horizontal walls and two vertical walls at temperatures T_h and T_c. This problem again has been a classical natural convection problem for decades, but most studies are based on the incompressible formulation with the Boussinesq approximation [26], which is appropriate only for a small temperature difference between the vertical walls. Practical applications such as furnace or nuclear reactor design, however, require much larger temperature differences so that compressible formulations without the Boussinesq approximation must be employed. For this reason, this problem is chosen as representative of a group of low-speed flows that are compressible because of density changes induced by surface heat transfer. It is known that this problem exhibits complex flow features depending on the Rayleigh number ($Ra = \rho^2 g\beta(T_h - T_c) L^3 C_p/\mu k$), the aspect ratio, and a temperature difference parameter ($\varepsilon = (T_h - T_c)/(T_h + T_c)$). Here β is the thermal expansion coefficient and L is the enclosure length. For the present study, three Rayleigh number cases, $Ra = 10^3$, 10^5, and 10^6 are considered with a temperature difference parameter $\varepsilon = 0.6$. The aspect ratio of the present problem is one and transport properties (μ and k) are evaluated by using Sutherland's law. The Prandtl number based on reference transport properties is 0.7. A 61×61 uniform grid is used for $Ra = 10^3$, and a 91×91 uniform grid is used for $Ra = 10^5$ and 10^6. Convergence rates with preconditioning for the three cases are shown in Fig. 19. In all cases, convergence behaviors are essentially the same and 300 steps are required for one order of magnitude drop of $\Delta Q/Q$.

Figure 20 shows streamline and temperature isolines for $Ra = 10^3$, 10^5, and 10^6. It is well known that solutions with

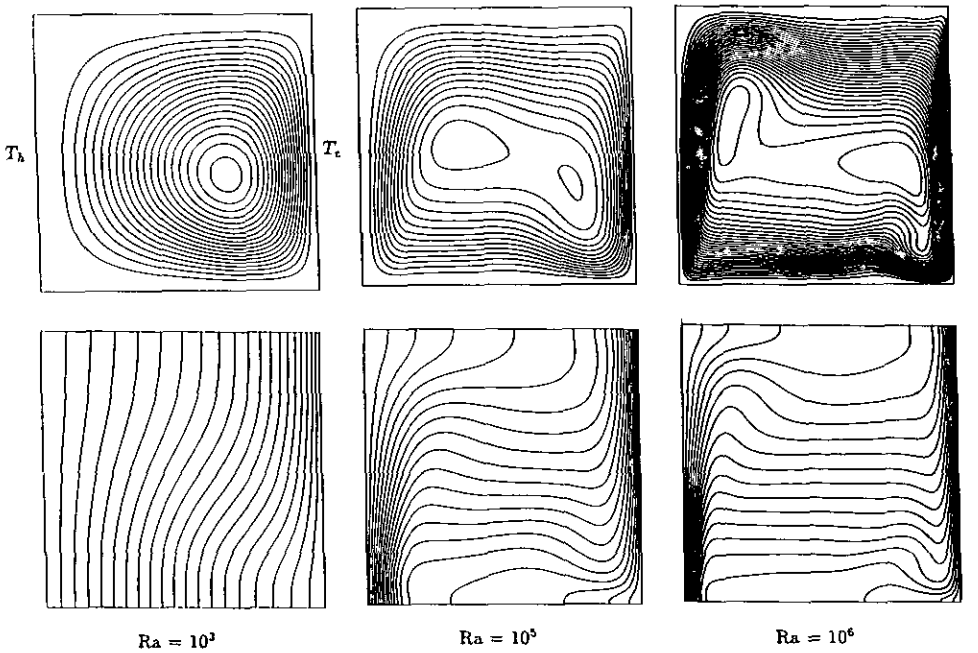

FIG. 20. Streamline and isoline temperature contours for a viscous flow in a thermally driven cavity for $Ra = 10^3$, 10^5 and 10^6.

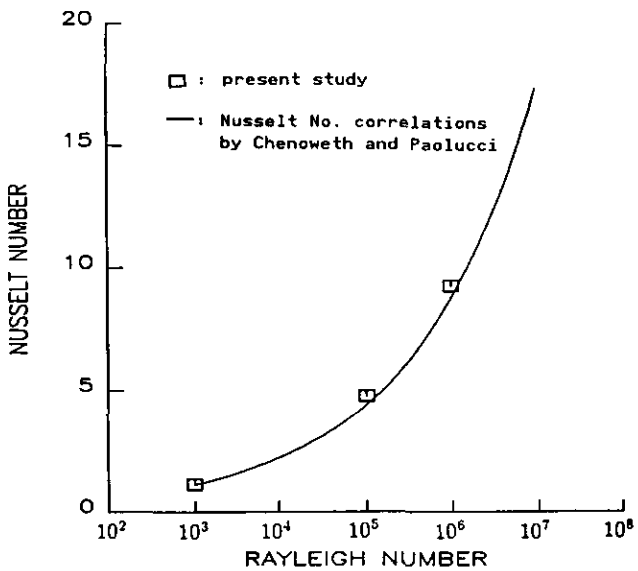

FIG. 21. Comparison of Nusselt number with a correlation by Chenoweth and Paolucci [18].

the Boussinesq approximation display a fully antisymmetric flowfield with respect to the center of the enclosure and miss the experimentally observed asymmetries. The present results based on the full equations show a pronounced difference with increasing temperature differences and a flowfield that is asymmetric as desired. At $\mathrm{Ra} = 10^3$, a shift of the center of the vortex towards the cold wall and downwards to the lower wall of the enclosure is manifest. In all cases, the basic form of the flowfield is a recirculating roll. This recirculation is driven by the generation of vorticity by the horizontal temperature gradient $(\partial T/\partial x)$. At $\mathrm{Ra} = 10^3$, $\partial T/\partial x$ is negative over the entire flowfield and a single primary clockwise rotating roll is formed. At $\mathrm{Ra} = 10^5$ and 10^6, there are two secondary rolls embedded in the single roll base flow. These secondary rolls are generated because at high Ra numbers the intense development of the thermal boundary layers in the vicinity of the wall leads to sign reversal for the temperature gradient $\partial T/\partial x$. Also it can be noted that as Ra increases, the secondary rolls intensify and their centers move towards the side walls. The accuracy of numerical solutions is verified by comparing the Nusselt number at the left side wall with a correlation by Chenoweth and Paolucci [18] in Fig. 21. Good agreement can be observed for all three cases.

6. SUMMARY

Extension of a time-derivative preconditioning method to viscous flows has been considered. A previously developed preconditioning method fails in viscous flows because of nonphysical time reversal for diffusive terms. In order to circumvent difficulty in the diffusion terms, the equations are first transformed to a "viscous" set of primary dependent variables before the preconditioning matrix is developed. With these primary dependent variables, the equations degenerate to the classical diffusion equations in the limit of highly diffusive flows. The proper scaling of the time derivatives is made to obtain well-conditioned eigenvalues for efficient convergence in inviscid flows. The resulting algorithm also provides a mechanism for keeping both the von Neumann number and the CFL number of order one at very viscous conditions, thereby ensuring rapid convergence at low Reynolds numbers. Because the preconditioning matrix operates only on the left-hand side of the discretized equations and central differences (with unsplit flux vectors) are used, the resulting solutions with preconditioning are identical to those without. Roundoff error which has a significant effect below $M = 10^{-3}$ has also been addressed and avoided by employing a gauge pressure. The quantitative effects of the new preconditioning method on the convergence of a time-marching algorithm have been investigated for several types of problems. Comparisons with previous results have verified the accuracy of these solutions. The convergence enhancement obtained with the preconditioning matrix ranges from a factor of two to several orders of magnitude. It is shown that low Mach number preconditioning provides excellent convergence even when the flowfield contains transonic regions whose stiffness is not counteracted by the preconditioning.

ACKNOWLEDGMENTS

This work is sponsored by NASA Lewis Research Center under Contract NAS3-25266 with Bernard J. Blaha as project manager and by NASA Grant NAGW-1356 Supplement 3.

REFERENCES

1. J. S. Sovey, T. L. Hardy, and M. Englehart, NASA TM-86998, 1986.
2. H. Viviand, *Numerical Methods for the Euler Equations of Fluid Dynamics*, edited by F. Angrand *et al.* (SIAM, Philadelphia, 1985).
3. R. Peyret and H. Viviand, *Recent Advances in the Aerospace Sciences*, edited by C. Casci, (Plenum, New York, 1985).
4. E. Turkel, *J. Comput. Phys.* **72**, 277 (1987).
5. B. van Leer, C.-H. Tai, and K. G. Powell, AIAA Paper 89-1933, 1989.
6. M. A. Storti, C. E. Baumann, and S. R. Idelsohn II, WCCM, Stuttgart, 1990.
7. W. R. Briley, H. McDonald, and S. J. Shamroth, *AIAA J.* **21**, 1467 (1983).
8. D. Choi and C. L. Merkle, *AIAA J.* **23**, 1518 (1985).
9. Y.-H. Choi, Ph.D. thesis, Pennsylvania State University, University Park, PA, 1989 (unpublished).
10. J. Feng and C. L. Merkle, AIAA Paper 90-0016, 1990.
11. J. F. Dannenhoffer III and M. B. Giles, *AIAA J.* **28**, 1457 (1990).
12. C. L. Merkle and Y.-H. Choi, *Int. J. Numer. Methods Eng.*, **25** 293 (1988).
13. J. Guerra and B. Gustafsson, *J. Comput. Phys.* **63**, 377 (1986).

14. S. Venkateswaran, C. L. Merkle, and S. T. Thynell, *J. Propulsion Power* **8**, 541 (1992).
15. A. Hosangadi, C. L. Merkle, and S. R. Turns, *AIAA J.* **28**, 1473 (1990).
16. J. P. Withington, J. S. Shuen, and V. Yang, AIAA Paper 91-0581, 1991.
17. R. G. Rehm and H. R. Baum, *J. Res. Nat. Bur. Stand.* **83**, 297 (1978).
18. D. R. Chenoweth and S. Paolucci, *J. Fluid Mech.* **169**, 173 (1986).
19. P. A. McMurtry, W. H. Jou, J. J. Riley, and R. W. Metcalfe, *AIAA J.* **24**, 962 (1986).
20. G. Volpe, AIAA Paper 91-1662, 1991.
21. J. Douglas and J. E. Gunn, *Numer. Math* **6**, 428 (1964).
22. R. F. Warming, and R. M. Beam, *Computational Fluid Dynamics*, edited by H. B. Keller, Amer. Math. Soc., Providence, RI, 1978, p. 85.
23. A. S. Grove, F. H. Shair, E. E. Petersen, and A. Acrivos, *J. Fluid Mech.* **19**, 60 (1964).
24. B. Fornberg, *J. Fluid Mech.* **98**, 819 (1980).
25. U. Ghia, K. N. Ghia, and C. T. Shin, *J. Comput. Phys.* **48**, 387 (1982).
26. W. M. Kayes and M. E. Crawford, *Convective Heat and Mass Transfer*, 2nd ed. (McGraw-Hill, New York, 1980).